Mie scattering in the time domain. Part 1. The role of surface waves

James A. Lock[1,*] and Philip Laven[2]

[1]*Department of Physics, Cleveland State University, Cleveland, Ohio 44115, USA*
[2]*9 Russells Crescent, Horley RH6 7DJ, United Kingdom*
**Corresponding author: j.lock@csuohio.edu*

Received February 15, 2011; accepted March 16, 2011;
posted April 4, 2011 (Doc. ID 142610); published May 18, 2011

We computed the Debye series $p = 1$ and $p = 2$ terms of the Mie scattered intensity as a function of scattering angle and delay time for a linearly polarized plane wave pulse incident on a spherical dielectric particle and physically interpreted the resulting numerical data. Radiation shed by electromagnetic surface waves plays a prominent role in the scattered intensity. We determined the surface wave phase and damping rate and studied the structure of the $p = 1, 2$ surface wave glory in the time domain.

OCIS codes: 290.1350, 290.4020, 320.2250.

1. INTRODUCTION

Lorenz–Mie theory provides the exact solution for the scattering of a monochromatic electromagnetic plane wave by a spherical particle in the form of an infinite series of partial wave contributions [1–3]. Although the solution is exact, it is not readily interpretable in terms of intuitive and familiar scattering processes in the short wavelength limit. This difficulty is partially remedied by the Debye series decomposition of the partial wave scattering amplitudes a_n and b_n into a series of contributions corresponding to diffraction, specular reflection, transmission, and transmission following $p - 1$ internal reflections of the partial waves, where n is the partial wavenumber and $p = 0, 1, 2, \ldots$ [4,5].

There are a number of scattering processes that are not separated by the Debye series, such as morphology-dependent resonances [6], which require the cooperation of a large number of Debye series terms in order to produce the phenomenon. Such processes are not examined in this study. Another class consists of two or more geometrical ray contributions at the same scattering angle that occurs in the same Debye series term. Examples of this for $p = 2$ are the two rays whose scattering angle is slightly larger than the Descartes rainbow angle and produce the supernumerary interference pattern [7]. Another $p = 2$ example for a sphere with refractive index greater than $\sqrt{2}$ is the central ray and the large impact parameter ray, which are both backscattered. In these two examples, the two scattered rays superpose either constructively or destructively in the far zone, and their existence can be inferred from the details of their angular interference pattern. In general, two rays in the same Debye series term with the same scattering angle have different length paths from the sphere's entrance plane to its exit plane. Thus, they can be resolved if a short electromagnetic pulse is incident on the sphere and the delay time is measured from when the incident pulse crosses the entrance plane to the arrival of the scattered pulses at the detector.

Most previous time-domain studies examined the Mie scattered intensity as a function of time at a single angular position and were mainly interested in applications of this technique to optical particle sizing [8–12]. In this paper, we examine the signature of various scattering processes in the time domain when only a single Debye series term is used, rather than the entire Mie scattering sum and when the time-domain intensity is plotted as a function of both scattering angle and delay time [13]. This provides a new tool with which to examine the details of a number of physical processes that were not amenable to careful numerical study using the Debye series alone or by making temporal measurements at only one scattering angle. Previous time-domain studies recognized the importance of the radiation shed by electromagnetic surface waves [14]. Thus, our main focus in this paper is a careful assessment of surface wave effects in the time domain. The body of this paper is organized as follows. In Section 2, we outline the calculation of the time-domain intensity for two incident pulse shapes and interpret the features of the intensity for the Debye series term for $p = 1$, corresponding to transmission through the sphere, and for $p = 2$, corresponding to transmission following one internal reflection. In Section 3, we determine the phase of the $p = 1$ surface wave scattered field, the angular damping rate of the $p = 2$ surface wave, and the details of the $p = 1$ surface wave glory. Lastly, in Section 4, we summarize our principal results. The time-domain analysis of the $p = 0$ Debye term describing diffraction, specular reflection, and grazing plus tunneling reflection is presented in a companion paper [15].

2. SCATTERING IN THE TIME DOMAIN

We consider an incident electromagnetic plane wave pulse traveling in the z direction with the dominant wavenumber k_0 and linearly polarized in the x direction. Its electric field magnitude and phase may be Fourier expanded as

$$E^{\text{pulse}}(z, t) = \int_{-\infty}^{\infty} (\mathrm{d}k/2\pi) A(k) \exp[\mathrm{i}k(z - ct)]. \tag{1}$$

If Mie scattering field response in the far zone at the angle θ to an incident plane wave with wavenumber k and unit field

strength is $E^{\mathrm{Mie}}(k,\theta)$, the far-zone time-domain scattered field is [16–18]

$$E^{\mathrm{scatt}}(t,\theta) = \int_{-\infty}^{\infty} (\mathrm{d}k/2\pi) A(k) E^{\mathrm{Mie}}(k,\theta) \exp(-\mathrm{i}ckt). \quad (2)$$

For the computational results described in this paper, we used the raised cosine pulse

$$\mathbf{E}^{\mathrm{pulse}}(z,t) = E_0 \cos^2[\pi(z-ct)t/2c\tau] \exp[\mathrm{i}k_0(z-ct)]\mathbf{u}_{\mathbf{x}} \quad (3)$$

for $-\tau \le t \le \tau$. The dominant wavelength and wavenumber are $\lambda_0 = 0.65\,\mu\mathrm{m}$ and $k_0 = 9.67 \times 10^6\,\mathrm{m}^{-1}$. After Fourier transforming a pulse with $\tau = 10\,\mathrm{fs}$ to a wavenumber space to obtain $A(k)$, we then truncated $|A(k)|^2$ at 10^{-4} of its peak value, giving the frequency band $6.74 \times 10^6\,\mathrm{m}^{-1} \le k \le 12.6 \times 10^6\,\mathrm{m}^{-1}$. Inverse Fourier transforming the truncated spectrum back to the time domain, the resulting truncated pulse was found to be virtually the same as the original pulse for $-\tau \le t \le \tau$, but possessed weak sideband oscillations for $t < -\tau$ and $t > \tau$ with an amplitude less than $10^{-5}E_0$.

For ease in performing various integrals analytically in this paper, we used the Gaussian pulse shape

$$\mathbf{E}^{\mathrm{pulse}}(z,t) = E_0 \exp[-(z-ct)^2/\sigma^2] \exp[\mathrm{i}k_0(z-ct)]\mathbf{u}_{\mathbf{x}}, \quad (4)$$

giving

$$A(k) = \sigma E_0 (\pi)^{1/2} \exp[-\sigma^2(k-k_0)^2/4], \quad (5)$$

where the temporal pulse width is parameterized by σ. A time interval of 10 fs between the $E = 0.5E_{\max}$ points, as in the raised cosine pulse of Eq. (3), corresponds to $\sigma = 18.01 \times 10^{-7}\,\mathrm{m}$. But if the wavenumbers $6.74 \times 10^6\,\mathrm{m}^{-1}$ and $12.6 \times 10^6\,\mathrm{m}^{-1}$ are chosen to be at the 10^{-4} points of $|A(k)|^2$, then $\sigma = 14.65 \times 10^{-7}\,\mathrm{m}$. Thus, the value of σ for the Gaussian pulse varies by about 25% when fitting different properties of the raised cosine pulse.

We can straightforwardly determine the features of geometrical ray scattering in the time domain. For a collection of initially parallel rays making a given number of internal reflections within the sphere, the magnitude and phase of the scattered field in some appropriate angular interval takes the form

$$E^{\mathrm{ray}}(k,\theta) = kaB(\theta) \exp[\mathrm{i}ka\Phi(\theta)], \quad (6)$$

where $kaB(\theta)$ is the field amplitude, $ka\Phi(\theta)$ is the phase, and the $E_0[\exp(ikr - i\omega t)]/(kr)$ dependence of the outgoing spherical wave has been suppressed. Substituting Eq. (6) and the Gaussian pulse of Eq. (5) into Eq. (2) and evaluating the integrals analytically, the magnitude squared of the time-domain field is the intensity

$$I^{\mathrm{ray}}(t,\theta) = (k_0 a)^2 B^2(\theta) \exp\{-2[ct - a\Phi(\theta)]^2/\sigma^2]\}, \quad (7)$$

where the $E_0^2/(k_0 r)^2$ dependence has again been suppressed. The temporal Gaussian dependence reaches its peak value at

$$t = a\Phi(\theta)/c, \quad (8)$$

which is identical to the case of monochromatic plane wave incidence since Eq. (8) is also the relation between the time delay of a monochromatic scattered ray and its phase. The angular dependence of the temporal ray intensity peak is also identical to that for scattering by a monochromatic plane wave of wavenumber k_0.

In order to computationally validate these ray predictions, Fig. 1 shows a false color graph of the computed Mie theory time-domain scattered intensity as a function of the delay time t and scattering angle θ for the raised cosine pulse of Eq. (3) with the pulse parameters described earlier. The pulse is incident on a spherical water droplet of radius $a = 10\,\mu\mathrm{m}$ and complex refractive index $N + \mathrm{i}K = 1.3326 + \mathrm{i}(1.67 \times 10^{-8})$ in a vacuum [19,20]. Dispersion of the refractive index of water over the pulse's frequency band has been neglected. The scattered field was obtained for a large number of evenly spaced wavenumbers in the frequency interval, and was converted to the time domain using the FFT algorithm. The magnitude squared of the time-domain electric field was plotted at time intervals of $\Delta t \approx 0.54\,\mathrm{fs} = \lambda_0/4c$ in Fig. 1, and the detector integration time has not been taken into account. The delay times given in Fig. 1 are relative to that of specular reflection of the central ray at $\theta = 180°$.

The false color graph in Fig. 2 shows the results of Debye series calculations, showing only the $p = 1$ term. The ray theory prediction for the $p = 1$ transmission scattering angle as a function of the delay time is given parametrically by

$$\theta = 2\theta_i - 2\theta_t, \quad (9)$$

$$t = 2a[1 - \cos(\theta_i)]/c + 2aN\cos(\theta_t)/c, \quad (10)$$

$$\sin(\theta_{\mathrm{i}}) = N\sin(\theta_{\mathrm{t}}), \quad (11)$$

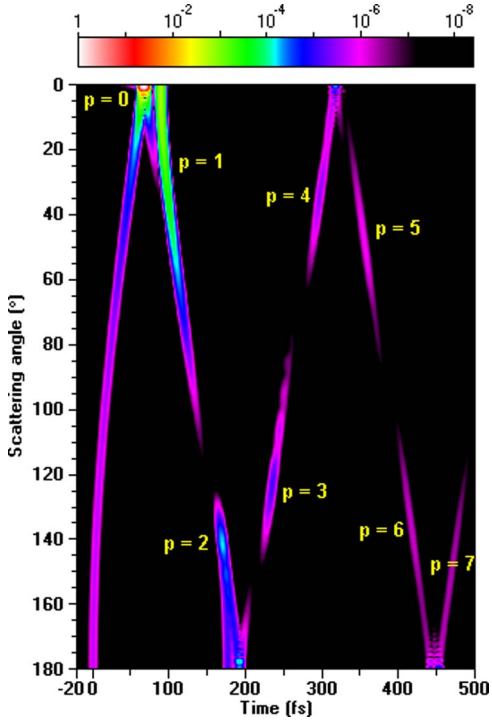

Fig. 1. (Color online) Scattered intensity in the time domain calculated using Mie theory as a function of the delay time t and scattering angle θ for a raised cosine pulse with $k_0 = 9.67 \times 10^6\,\mathrm{m}^{-1}$ and $\tau = 5\,\mathrm{fs}$ incident on a spherical particle of radius $a = 10\,\mu\mathrm{m}$ and refractive index $1.3326 + \mathrm{i}(1.67 \times 10^{-8})$.

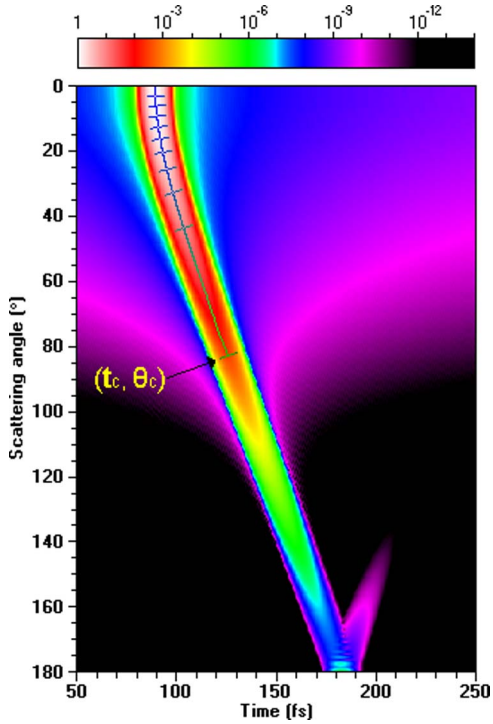

Fig. 2. (Color online) $p = 1$ component of the scattered intensity in the time domain as a function of the delay time t and scattering angle θ for the pulse and particle parameters of Fig. 1. The false color scale for intensity in Fig. 1 has been reset in Fig. 2 to emphasize the low-intensity components. The ray theory scattering angle as a function of delay time of Eqs. (9)–(11) has been overlaid on the figure. The grid ticks on the ray theory line correspond to the ray impact parameter b in intervals of $\Delta b = 0.1$.

for the range of angles of incidence $0° \le \theta_i \le 90°$, and has been overlaid on the figure. The scattering angle monotonically increases as a function of the ray impact parameter. The central ray $\theta_i = 0°$ is scattered at $\theta = 0°$ and $t = 88.84$ fs. The grazing incidence ray at $\theta_i = 90°$ is the last ray to strike the sphere. It is classically transmitted into the sphere with zero intensity and exits at the critical scattering angle $\theta_c = 82.75°$ and $t_c = 125.39$ fs. The time-domain signal in Fig. 2, however, extends far beyond that of grazing ray incidence and can be understood as follows. In wave theory, the edge region for scattering consists of partial waves with $n + 1/2 = ka + \varepsilon(ka)^{1/3}, -\varepsilon_{\max} \le \varepsilon \le \varepsilon_{\max}$ and $\varepsilon_{\max} \approx 4.05$ [21]. It corresponds to geometrical rays that either strike the sphere with grazing incidence or classically just miss striking the sphere but nonetheless tunnel through the centrifugal barrier surrounding it and weakly interact with the sphere [22]. The interaction of these partial waves with the sphere produces electromagnetic surface waves that propagate along the sphere surface and are angularly damped as they shed radiation tangent to the sphere into the far-zone beginning at the ray optics boundary θ_c. The smooth transition between the geometrical ray scattered field for $\theta \ll \theta_c$ and the surface wave region for $\theta \gg \theta_c$ is known as the Fock transition [23], whose angular width is approximately $1.5(2/ka)^{1/3} \approx 24°$ to each side of center. The extension of the time-domain intensity of Fig. 2 past t_c is due initially to the Fock transition, and then afterward to the radiation shed by surface waves. The four surface wave contributions to the $p = 1$ scattered field for $\theta \approx 180°$ are illustrated in Fig. 3. Paths A and B contribute to the scattered field at angles slightly less than 180° as measured clockwise from the forward direction. Similarly, paths C and D contribute at angles slightly larger than 180°. Together, they interfere to produce the $p = 1$ surface wave glory, which is evident in the time domain by the crossing of the surface wave arms in Fig. 4.

Similarly, Fig. 5 shows a false color graph of the computed $p = 2$ Debye series time-domain intensity as a function of t and θ for the same pulse and sphere parameters. It illustrates

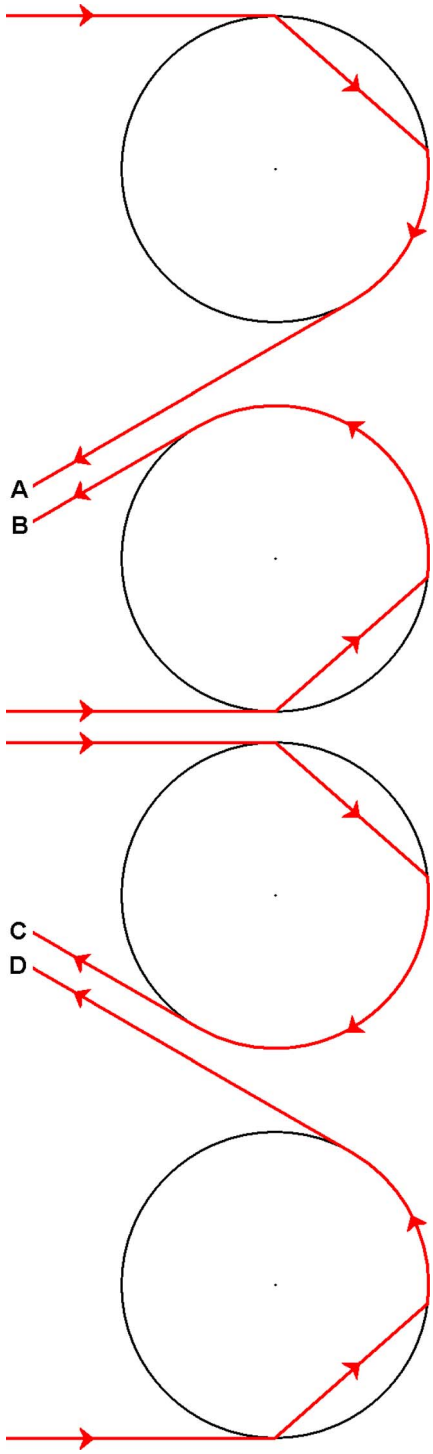

Fig. 3. (Color online) Pictorial representation of the $p = 1$ surface waves A and B with $\theta < 180°$, and C and D with $\theta > 180°$. A and D are the short path length surface waves, and B and C are the long path length surface waves.

the effects of partial waves that have been transmitted out of the sphere following one internal reflection. Again, the ray theory prediction for the scattering angle as a function of delay time,

$$\theta = \pi + 2\theta_i - 4\theta_t, \tag{12}$$

$$t = 2a[1 - \cos(\theta_i)]/c + 4aN\cos(\theta_t)/c, \tag{13}$$

has been overlaid on the graph. The central ray $\theta_i = 0°$ is scattered at $\theta = 180°$ and $t = 177.68$ fs, and the grazing incidence ray $\theta_i = 90°$ is scattered at $\theta_c = 165.50°$ and $t_c = 184.11$ fs. The Descartes rainbow ray is $\theta_R = 137.86°$ and $t_R = 168.37$ fs. In Fig. 5, two rays for each scattering angle in the interval $\theta_R < \theta < \theta_c$ interfere with each other to produce the supernumerary bows when the scattered intensity is graphed as a function of θ for a single incident wavelength. But Fig. 5 shows that the contributions from the two rays are separated in the time domain. As was the case for $p = 1$, the time-domain intensity for delay times larger than t_c corresponds initially to the Fock transition, and then afterward to the contribution of surface waves. The $p = 2$ surface wave glory with the ray theory time delay $t = 192.54$ fs also prominently appears in the figure.

3. SURFACE WAVES IN THE TIME DOMAIN

A. Phase of the p=1 Surface Wave Radiation

For $p = 1$ scattering in the short wavelength limit at angles $\theta \ll \theta_c$, the Mie–Debye sum over partial waves produces

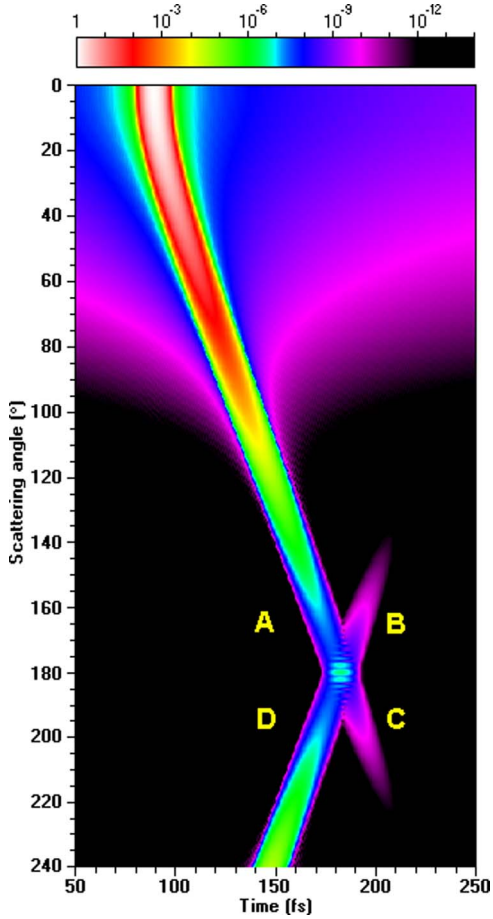

Fig. 4. (Color online) Similar to Fig. 2, but also showing scattering for $\theta > 180°$. The surface waves A + C and D + B of Fig. 3 intersect at $\theta = 180°$ to form the $p = 1$ surface wave glory.

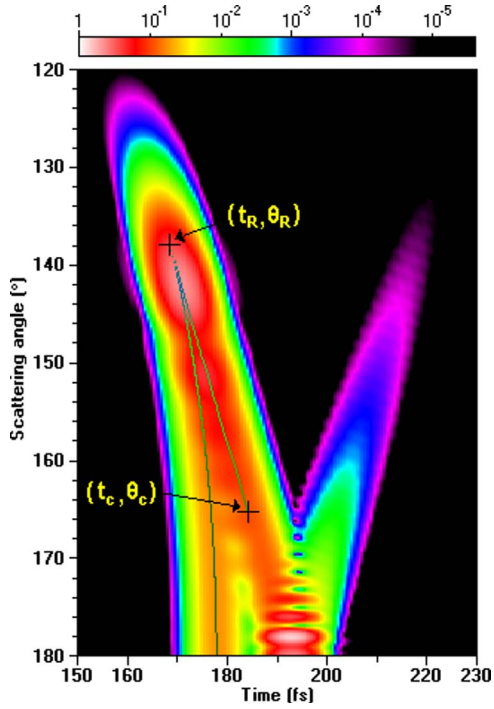

Fig. 5. (Color online) $p = 2$ component of the scattered intensity in the time domain as a function of the delay time t and scattering angle θ for the pulse and particle parameters of Fig. 1. The ray theory scattering angle as a function of delay time of Eqs. (12) and (13) has been overlaid on the figure.

the transitional approximation to the geometrical optics fields in the following way. The Riccati–Bessel and Riccati–Neumann functions appearing in the partial wave scattering amplitudes a_n and b_n are approximated by their large-argument, large-order asymptotic expansions [24]. The angular functions $\pi_n(\theta)$ and $\tau_n(\theta)$ for θ away from 0° and 180° are expanded in powers of $n + 1/2$ and the leading term is retained [25]. The sum over partial waves $1 \le n \le ka - \varepsilon_{max}(ka)^{1/3}$ corresponding to geometrical rays striking the sphere surface below the edge region is approximated by an integral over an effective impact parameter [26,27]. The integral is then evaluated using the method of stationary phase [28]. On the other hand, for scattering at $\theta \gg \theta_c$ and θ away from 180°, the surface wave field is obtained for partial waves in the edge region by using the large-argument, large-order asymptotic expansion of the partial wave scattering amplitudes [29] and retaining the leading term in the expansion of the resulting partial wave scattering amplitudes in powers of $1/ka$. The first term in the expansion of the angular functions in powers of $n + 1/2$ is also used. The resulting sum over partial waves is approximated by an integral over ε, which is then extended to a contour integral in the complex plane and is evaluated using the method of residues [23]. The contribution of the dominant pole of the integrand in the complex plane is

$$\mathbf{E}^{\text{surface waves}}(\theta) = (ka)^{5/6}[-T_2(\theta)B_2(k,\theta)\cos(\varphi)\mathbf{u}_\theta + T_1(\theta)B_1(k,\theta)\sin(\varphi)\mathbf{u}_\varphi]\exp[ika\Phi(k,\theta)]. \tag{14}$$

In Eq. (14), the portion of the field magnitude that is independent of k is

$$T_j(\theta) = \exp(\mathrm{i}\pi/12)2^{1/6}K_j\xi/\{[\pi(N^2-1)\sin(\theta)]^{1/2}[\mathrm{Ai}'(-X)]^2\}, \quad (15)$$

the portion of the magnitude that depends on k is

$$B_j(k,\theta) = \exp\{-\xi[3^{1/2}X(ka)^{1/3}/2^{4/3} - K_j/(N^2-1)^{1/2}]\}, \quad (16)$$

and the phase is $ka\Phi(\theta)$ with

$$\Phi(k,\theta) = 2 + 2(N^2-1)^{1/2} + \xi\{1 + X/[2^{4/3}(ka)^{2/3}]\}. \quad (17)$$

In Eqs. (15)–(17),

$$\xi = \theta - \theta_c \quad (18)$$

and $X = 2.3381$ is the magnitude of the argument of the first zero of the Airy function [30], which occurs in the residue of the dominant pole of the integrand. The polarization dependence is given by $K_\mathrm{j} = 1$ for $\mathrm{j} = 1$, the TE or perpendicular polarization, and $K_\mathrm{j} = N^2$ for $\mathrm{j} = 2$, the TM or parallel polarization. The factor of $(ka)^{5/6}$ in Eq. (14) indicates that the strength of the surface waves is below that of the ray optics background of Eq. (6). The transitional approximation to the surface wave field of Eq. (14) can be made more accurate by including higher-order Taylor series contributions to Eqs. (15)–(17) and by including the residues of a larger number of poles of the integrand in the complex plane (22), (23), and (28). A more accurate (but more complicated) uniform approximation to the scattered field was considered in [31,32].

One of the goals of this study is to assess the accuracy of Eqs. (14)–(17). Although this may be done for either a single incident monochromatic plane wave or an incident plane wave pulse in the time domain, we now show that the time-domain analysis provides an interesting approach to the determination of the surface wave velocity. We consider the beam and particle parameters $p = 1$, $\lambda = 0.65\,\mu$m, $a = 10\,\mu$m, and $N + \mathrm{i}K = 1.3326 + \mathrm{i}(1.67\times10^{-8})$. First, the $p = 1$ portion of the scattered electric field for unpolarized monochromatic plane wave incidence was calculated for a dense grid of scattering angles in the surface wave region. We then determined $ka(\Delta\Phi/\Delta\theta)$, the change in the phase of the scattered field per degree of change in scattering angle. If the surface wave acquires phase at an angular rate faster than if it were traveling on the sphere surface at the speed of light, its effective velocity v on the sphere surface would be given by

$$v/c = (\Delta\Phi/\Delta\theta)^{-1} < 1. \quad (19)$$

The results for monochromatic plane wave incidence are shown as the blue lines in Fig. 6. The quantity v/c monotonically decreases for $\theta < 120°$ in the angular regime of the Fock transition; it is slowly varying with the value $v/c \approx 0.96$ in the narrow angular region $120° < \theta < 140°$ of surface wave dominance, and it becomes increasingly oscillatory for $\theta > 140°$ in the angular regime of interfering counterpropagating surface waves. This agrees well with the theoretical prediction of Eq. (17):

$$(\Delta\Phi/\Delta\theta)^{-1} = \{1 + X/[2^{4/3}(ka)^{2/3}]\}^{-1} = 0.958. \quad (20)$$

The agreement is noteworthy, considering the narrowness of the angular region in which $(\Delta\Phi/\Delta\theta)^{-1}$ is only very roughly constant.

The quantity v/c can also be measured in the time domain. Referring to Fig. 2 for $p = 1$, the slope of the graph multiplied by the sphere radius gives the effective velocity of the surface wave. We thus determined v/c in the time domain in the following way. For each θ in 5° increments in the interval $80° \le \theta \le 180°$ and for the time interval pixel width $\Delta t = 0.54$ fs, the temporal peak of the time-domain curve was determined to subpixel accuracy by fitting the four data points nearest the temporal intensity peak with a cubic function and then differentiating to find the peak position. The slopes were then determined and then the least-squares fit, giving $v/c = 0.9827$. The same procedure was also applied to the $p = 2$ time-domain graph of Fig. 5 in $\Delta\theta = 1°$ increments for $190° \le \theta \le 300°$ and gave $v/c = 0.9850$. These results, at first appearance, are in seemingly poor agreement with the theoretical prediction of Eq. (20). In attempting to find the reason for the difference, we decreased the $p = 1$ time interval pixel width by a factor of 128 to $\Delta t \approx 0.004$ fs and repeated the fitting procedure. The results are graphed as the red (top) curves in Fig. 6, which show (i) decreasing v/c in the Fock transition region, (ii) a much wider and flatter plateau in the surface wave region with $v/c \approx 0.9840$, and (iii) an increasing oscillatory structure in the region of counterpropagating surface wave interference. The same procedure was applied to each polarization individually with similar results. The result still seemingly differs from Eq. (20) despite the fact that v/c in the time domain is more nearly constant over a substantially larger angular interval than it was for monochromatic plane wave incidence.

The difference is due to the relatively wide wavenumber spectrum of the pulse. Since the function $\Phi(k,\theta)$ of Eq. (17) is not independent of k, the surface wave speed depends weakly on k. When one has a pulse with a spectrum of different k values, one adds together Fourier components whose speeds are both slightly slower and slightly faster than average. But the effect is not symmetric about k_0. Thus, when the uneven mix of faster and slower surface wave speeds are averaged together over the spectrum, the final effective surface wave speed is shifted from what it was for k_0 alone. This can be demonstrated mathematically as follows. Substituting Eqs. (5) and (14) into Eq. (2), the time-domain scattered field is

$$E_j^{\mathrm{scatt}}(t,\theta) = [\sigma T_j(\theta)/2\pi^{1/2}]\int_{-\infty}^{\infty}\mathrm{d}k\exp\{-[\sigma^2(k - k_0)^2/4]\}(ka)^{5/6}B_\mathrm{j}(k,\theta)\exp[\mathrm{i}ka\Phi(k,\theta) - \mathrm{i}ckt]. \quad (21)$$

Assuming $(ka)^{5/6}B_\mathrm{j}(k,\theta)$ with the implicit $1/kr$ dependence and $\Phi(k,\theta)$ are both slowly varying functions of k in the vicinity of k_0, their Taylor series expansions about k_0 can be written as

$$B_j(k,\theta) = B_{\mathrm{j}0}(k_0,\theta) + O(k-k_0), \quad (22)$$

$$\Phi(k,\theta) = \Phi_0(k_0,\theta) + (k-k_0)\Phi_1(k_0,\theta) + O[(k-k_0)^2]. \quad (23)$$

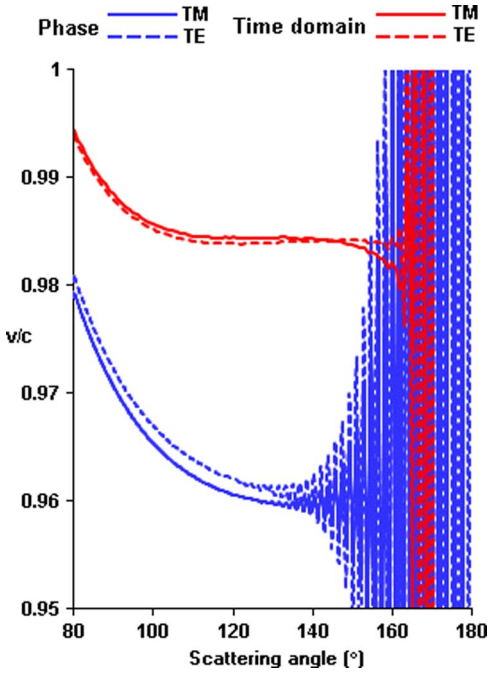

Fig. 6. (Color online) The quantity v/c, where v is the effective surface wave velocity on the sphere surface, as a function of the scattering angle θ obtained [blue (bottom) curves] from the angular advancement of the phase of the $p = 1$ component of the scattered field when a monochromatic plane wave with $k = 9.67 \times 10^6\ \mathrm{m}^{-1}$ is incident on a spherical particle with the parameters of Fig. 1, and from the temporal maximum of the $p = 1$ scattered pulse [red (top) curves]. The pulse and particle parameters are the same as in Fig. 1 except that the temporal pixel width is $\Delta t \approx 0.004\,\mathrm{fs}$.

If the phase were linear in k, i.e., if $\Phi(k,\theta)$ were independent of k, Φ_1 would vanish. Substitution into Eq. (21) gives

$$\begin{aligned} E_j^{\mathrm{scatt}}(t,\theta) = {} & [(k_0a)^{5/6}\sigma T_{\mathrm{j}}(\theta)B_{\mathrm{j}0}(k_0,\theta)/2\pi^{1/2}] \\ & \times \int_{-\infty}^{\infty} \mathrm{d}k \exp[-\sigma^2(k-k_0)^2/4] \\ & \times \exp\{\mathrm{i}ka[\Phi_0(k_0,\theta) + (k-k_0) \\ & \times \Phi_1(k_0,\theta) - \mathrm{i}ckt]\}, \end{aligned} \tag{24}$$

which can be integrated analytically. Multiplying the result by its complex conjugate, the time-domain intensity is

$$\begin{aligned} I_j^{\mathrm{scatt}}(t,\theta) = {} & (k_0a)^{5/3}[\sigma T_{\mathrm{j}}(\theta)B_{\mathrm{j}0}(k_0,\theta)/2]^2[(\sigma^2/4)^2 + (\Phi_1 a)^2]^{-1/2} \\ & \times \exp\{-2\sigma^2(ct - a\Phi_0 - k_0a\Phi_1)^2/ \\ & \times [(\sigma^2/4) + (\Phi_1 a)^2]\}. \end{aligned} \tag{25}$$

The Gaussian time dependence reaches its peak value at

$$ct = a\Phi_0 + k_0a\Phi_1, \tag{26}$$

indicating that the nonlinearity of the surface wave phase $ka\Phi(k)$, expressed via a nonzero value of Φ_1, shifts the peak of the time-domain intensity. For the magnitude and phase functions of Eqs. (16) and (17), we have

$$B_{\mathrm{j}0}(k_0,\theta) = \exp\{-\xi[3^{1/2}X(k_0a)^{1/3}/2^{4/3} - K_{\mathrm{j}}/(N^2-1)^{1/2}]\}, \tag{27}$$

$$\Phi_0(k_0,\theta) = 2 + 2(N^2-1)^{1/2} + \xi + \xi X/[2^{4/3}(k_0a)^{2/3}], \tag{28}$$

$$\Phi_1(k_0,\theta) = -(2/3)\xi X a/[2^{4/3}(k_0a)^{5/3}], \tag{29}$$

giving

$$v/c = \{1 + (1/3)X/[2^{4/3}(k_0a)^{2/3}]\}^{-1} = 0.9855, \tag{30}$$

which is in good agreement with the time-domain results obtained from Fig. 6.

If the $\mathrm{O}(k-k_0)$ term of $(ka)^{5/6}B_{\mathrm{j}}(k,\theta)/(kr)$ were evaluated and substituted into Eq. (24), the integral can also be evaluated analytically [33] and the temporal peak of the time domain intensity for a given θ is shifted to a slightly earlier time than predicted by Eq. (26). When the $\mathrm{O}[(k-k_0)^2]$ term of $\Phi(k,\theta)$ is also substituted into Eq. (24), an estimation of the value of the resulting integral produces a comparable shift to a slightly later time. These two corrections nearly cancel, and Eq. (30) is a reasonable estimate of the surface wave velocity. The value of $1 - v/c$ from Fig. 6 deviates from its value in Eq. (30) by 10%. As a test to see whether this difference is attributable to k_0a not being far enough into the short wavelength limit, we determined the time-domain maximum intensity when $a = 100\,\mu\mathrm{m}$ and $\Delta t = 0.54\,\mathrm{fs}$, and obtained $v/c = 0.99622$. Equation (30) for these conditions gives $v/c = 0.99685$, and the time-domain result for $1 - v/c$ now deviates from Eq. (30) by 20%. This deviation agrees almost exactly with the value for $a = 10\,\mu\mathrm{m}$ and the original temporal pixel width $\Delta t = 0.54\,\mathrm{fs}$. Since the difference appears not to be related to the value of k_0a, the contribution of less dominant poles in the integrand of the contour integral warrants further consideration [31]. Returning to Eq. (25), Φ_1 also broadens the temporal response for a given scattering angle. However, for the beam and particle parameters used here, the broadening is minimal since $(\Phi_1 a)^2 < 0.01(\sigma^2/4)^2$.

The fact that v/c differs from 1 does not necessarily imply that the speed of the surface wave on the sphere surface is a few percent less than c. One could claim instead that the surface wave travels at the speed of light slightly above the sphere surface [34] at the radius

$$r = a\{1 + X/[2^{4/3}(ka)^{2/3}]\} = a[1 + 0.928/(ka)^{2/3}]. \tag{31}$$

This interpretation may be motivated in the following way. For partial waves in the edge region, the near-zone scattered field is approximately proportional to the Riccati–Bessel function $\psi_{\mathrm{ka}}(kr)$, which is derived from the Bessel function $J_{\mathrm{ka}+1/2}(kr)$, which in turn is related to the Airy function $\mathrm{Ai}(-2^{1/3}z)$ when the order and argument are nearly equal [29], i.e.,

$$kr = (ka + 1/2) + z(ka + 1/2)^{1/3} \approx ka + z(ka)^{1/3} \tag{32}$$

with $ka \gg 1$. The Airy function reaches its peak value [30] not at $z = 0$, but rather at $2^{1/3}z \approx 1.02$, giving

$$r = a[1 + 0.810/(ka)^{2/3}], \tag{33}$$

which is in reasonably close agreement with Eq. (31).

It should finally be noted that, in [8], surface waves were qualitatively modeled as traveling along the sphere surface

for the entirety of their path, and the refractive index of the sphere surface was allowed to be variable. In order to match the computed time delay and the time delay predicted using this model, a value of the surface refractive index was obtained that was intermediate between that of the sphere interior and the exterior medium. A more mathematically detailed interpretation of the surface wave path that includes short cuts through the sphere, however, was presented and physically motivated in [22] and is used in this paper to interpret our results.

B. Magnitude of the $p = 2$ Surface Wave Radiation

Since the angular extent of the $p = 2$ surface wave region in Fig. 5 without the intrusion of the glory region is much larger than for $p = 1$ surface waves in Fig. 2, we examine here the angular damping rate of the $p = 2$ surface wave intensity. The derivation of the expression analogous to Eqs. (14)–(17) for the $p = 2$ surface wave proceeds exactly as for $p = 1$, except that the poles of the $p = 2$ integrand of the contour integral are of a higher order than for $p = 1$. The only change in Eqs. (14)–(17) made by this more complicated residue is that $T_j(\theta)$ is proportional to a mixture of ξ^2 and ξ rather than to ξ alone. This slightly changes its behavior for $\theta \approx \theta_c$ where the surface wave expression is dominated by the Fock transition, but it will not change the exponential attenuation for $\theta \gg \theta_c$. Since $(\Phi_1 a)^2 \ll (\sigma^2/4)^4$ and the resulting broadening of the time-domain response is minimal, a comparison of the magnitude squared of Eq. (14) with Eq. (25) shows that the value of the peak intensity as a function of θ in the time domain is identical to the value of the scattered intensity as a function of θ for monochromatic plane wave incidence. Thus, it should make no difference whether the surface wave damping rate is measured in the time domain or for monochromatic plane wave incidence.

The maximum time-domain intensity multiplied by $|\sin(\theta)|$ is graphed for $p = 2$ in Fig. 7 as a function of θ for the TE and TM polarizations. The intensity was multiplied by $|\sin(\theta)|$ in order to compensate for the geometrically expected $[\sin(\theta)]^{-1}$ dependence [35] in the vicinity of backscattering, leaving only the expected exponential attenuation of the surface wave radiation. The figure clearly shows the rainbow region for $140° < \theta < 160°$, the relative maxima and minima of the counterpropagating surface waves in the glory region for $175° < \theta < 185°$, the Fock transition between the rainbow and glory regions, and the exponentially damped surface wave region for $185° < \theta < 240°$. An indication that the Fock transition extends between the rainbow and the glory regions is provided by the fact that $I(t_{\max}, \theta)|\sin(\theta)|$ is not an exact continuation of the surface wave curve that began beyond the glory region.

According to Eq. (16), the TE surface wave intensity should fall off faster than for the TM surface wave intensity, and should decay as $\exp(-\Gamma_j \xi)$ where $\Gamma_1 = 0.2178$ per degree for TE and $\Gamma_2 = 0.1871$ per degree for TM. Similarly, the TM surface wave intensity should be larger than that of the TE surface wave intensity by a factor of $N^4 = 3.15$. The attenuation coefficients of Fig. 7 were determined to be $\Gamma_1 = 0.157$ per degree and $\Gamma_2 = 0.138$ per degree, which are each about 73% of the expected value, and the TM intensity is larger than the TE intensity by about a factor of 10. In order to see whether there is any refractive index dependence of the decay

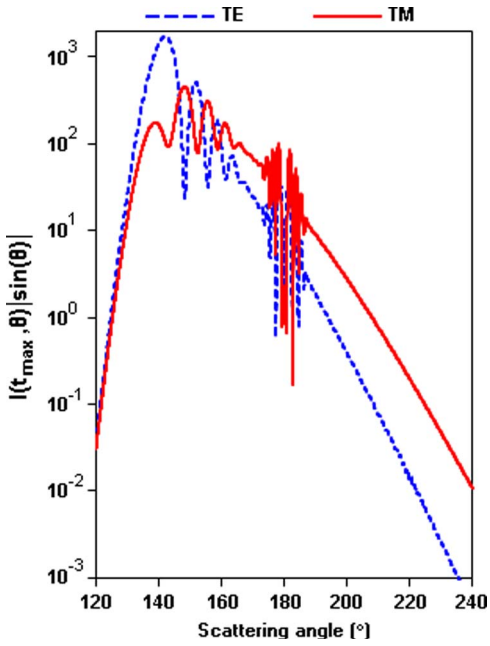

Fig. 7. (Color online) Maximum of the $p = 2$ intensity of the scattered pulse multiplied by $|\sin(\theta)|$ as a function of scattering angle θ for the pulse and particle parameters of Fig. 1.

rates, the maximum time-domain intensity was also computed for $a = 10\,\mu$m and $N = 1.5$. For this refractive index, Eq. (16) gives $\Gamma_1 = 0.2249$ per degree and $\Gamma_2 = 0.1859$ per degree, while the time-domain graph gives $\Gamma_1 = 0.165$ per degree and $\Gamma_2 = 0.132$ per degree. Again, each measured value is about 72% of the expected value. The difference between the obtained and expected damping rates and the TM/TE intensity ratio may be attributable to the fact that $k_0 a$ is not very far into the short wavelength limit.

C. $p = 1$ Surface Wave Glory

We have already seen in Fig. 4 that, for $p = 1$, the surface wave radiation region starts at about $\theta = 140°$, is interrupted by the surface wave glory region, and then continues again for $\theta > 180°$. This is readily visible in Fig. 8, which shows the $p = 1$ time-domain maximum intensity as a function of the scattering angle for the surface waves A and C. The damping rate of the surface waves is the same both below and above the glory region. There is, however, an asymmetry to the oscillations in the maximum intensity immediately above and below 180° in Fig. 8. This can be explained by Fig. 9, which is a fine-resolution view of Fig. 4 in the glory region. In Fig. 4, the short path length surface wave A arises out of the Fock transition for $\theta > \theta_c$, damps throughout the glory region, and continues to 200° and beyond as C. Similarly, the long path length surface wave D propagating in the opposite direction damps out from larger scattering angles and passes through the glory region to 160° and beyond as B. In Fig. 9, the less damped surface waves for smaller delay times are the left half of the "X"-shaped intersection and the more greatly damped surface waves for larger delay times are the right half. The counterpropagating surface waves of nearly equal strength interfere for $168° \le \theta \le 192°$, giving rise to the glory structure. Figure 9 also suggests the explanation of the observation of Fig. 8 that there is less interference structure for $\theta < 180°$ than there is for $\theta > 180°$. For $\theta < 180°$,

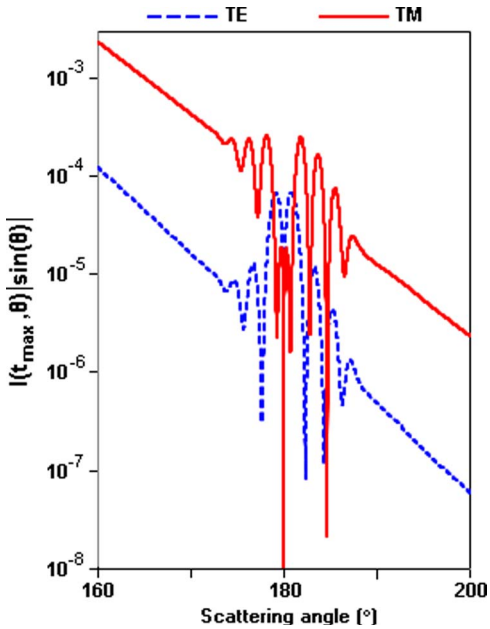

Fig. 8. (Color online) Maximum of the $p = 1$ intensity of the scattered pulse multiplied by $|\sin(\theta)|$ for the surface wave A + C of Fig. 3 as a function of the scattering angle θ for the pulse and particle parameters of Fig. 1. The maximum of surface wave A was determined for $\theta < 180°$, and the maximum of C was determined for $\theta > 180°$.

the center of the stronger short path length surface wave A superposes with the periphery of the weaker long path length surface wave B. As a result, their interference pattern has a relatively small modulation and extends over a relatively short angular interval. Following what used to be the shorter path length surface wave through the glory region to $\theta > 180°$, the center of the now weaker surface wave C superposes with the periphery of what is now the stronger surface wave D. Since the two wave amplitudes are comparable, their interference pattern has a large modulation and extends over a longer angular interval.

A sum over partial waves in the edge region must be performed in order to calculate the surface wave field in the glory region. As before, the partial wave scattering amplitudes are formed from the large-argument, large-order approximation to the Riccati–Bessel functions and Riccati–Hankel functions and the approximation [36] to the angular functions $\pi_n(\theta)$ and $\tau_n(\theta)$ appropriate near 180°. The leading term in the partial wave scattering amplitudes in powers of ka is retained, and the partial wave sum is approximated by an integral over an effective impact parameter, extended to a contour integral in the complex plane, and evaluated using the method of residues. Keeping only the contribution of the dominant pole of the integrand, one obtains

$$\mathbf{E}^{\text{scatt}}(\pi - \delta) = S_a(\pi - \delta)\mathbf{u}_\mathbf{x} - S_s(\pi - \delta) \times [\cos(2\varphi)\mathbf{u}_\mathbf{x} + \sin(2\varphi)\mathbf{u}_\mathbf{y}], \quad (34)$$

where $\theta = \pi - \delta$ and δ is a small angle. The scattering amplitudes are

$$S_a(\pi - \delta) = (ka)^{4/3}(N^2 - 1)\mathrm{J}_0(ka\delta)T(\pi - \delta)B(k, \pi - \delta)\exp[\mathrm{i}ka\Phi(k, \pi - \delta)], \quad (35)$$

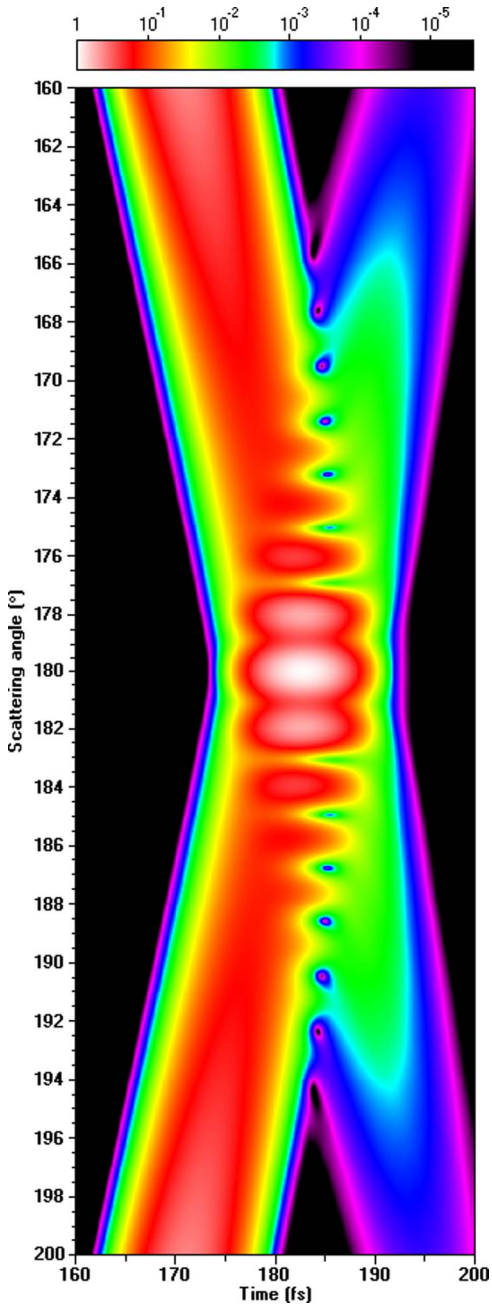

Fig. 9. (Color online) Fine-resolution view of Fig. 4 in the vicinity of the $p = 1$ surface wave glory region.

$$S_s(\pi - \delta) = (ka)^{4/3}(N^2 + 1)\mathrm{J}_2(ka\delta)T(\pi - \delta)B(k, \pi - \delta)\exp[\mathrm{i}ka\Phi(k, \pi - \delta)], \quad (36)$$

with

$$T(\pi - \delta) = \exp(-\mathrm{i}\pi/6)(\pi - \theta_c)/\{2^{1/3}(N^2 - 1)^{1/2}[\mathrm{Ai}'(-X)]^2\}, \quad (37)$$

$$B(k, \pi - \delta) = \exp\{-(\pi - \theta_c)[3^{1/2}X(ka)^{1/3}/2^{4/3} - (N^2 + 1)/2(N^2 - 1)^{1/2}]\}, \quad (38)$$

$$\Phi(k,\pi-\delta)=2+2(N^2-1)^{1/2}+(\pi-\theta_c)\{1+X/[2^{4/3}(ka)^{2/3}]\}. \tag{39}$$

Equation (38) has been simplified from that of [37] by replacing the different damping rates of the two polarizations by an average damping rate. Equations (37)–(39) are the glory region analogs of Eqs. (16)–(18) where the slower angular dependence on ξ in the surface wave attenuation factor and phase has been evaluated at $\pi-\theta_c$ and the more rapid angular dependence of the focusing functions $J_0(ka\delta)$ and $J_2(ka\delta)$ is retained. The factor of $(ka)^{4/3}$ in Eqs. (35) and (36) indicates that the radiation produced by surface waves in all planes of incidence constructively interferes at $\theta=180°$, producing partial focusing of the scattered field above the ray optics background of Eq. (6). It is amplified by a factor of $(ka)^{1/2}$ above the surface wave amplitude of Eq. (14) for angles below the glory region. The glory pattern of Eqs. (34)–(39) for electromagnetic scattering by a sphere is substantially more complicated than for scattering of scalar waves. It is an azimuthally dependent mixture of $J_0(k_0a\delta)$ and $J_2(k_0a\delta)$, whereas, for scalar wave scattering by a penetrable sphere, only $S_a(\pi-\delta)$ occurs, which is proportional to $J_0(k_0a\delta)$.

The largest relative maximum in Fig. 9 is centered on $t=182$ fs and $\theta=180°$ and is the main focusing peak of the Bessel function $J_0(k_0a\delta)$. When $k_0a\delta$ is greater than about 1.0, $J_0(k_0a\delta)$ may be approximated by its asymptotic form [38], which is proportional to $\exp[i(k_0a\delta-\pi/4)]+\exp[i(-k_0a\delta+\pi/4)]$. The physical interpretation of this replacement is related to the fact that $J_0(k_0a\delta)$ describes focusing. Its oscillatory behavior to either side of the central maximum is the alternate constructive and destructive interference of the shorter path length and longer path length surface waves to either side of the main focusing peak. When a geometrical light ray crosses a focal line, it acquires a non-path-length phase shift [39] of $-\pi/2$. This phase shift does not occur discontinuously at the focal line, but is the continual transition of the phase of the field from $\pi/4$ to $-\pi/4$ over the extent of the central peak of J_0, as is indicated in the asymptotic form of the Bessel function to either side of its central peak. This interpretation can be further motivated by approximating $J_0(x)$ with $\cos[x-\varphi(x)]$ and determining $\varphi(x)$ from the known numerical values of $J_0(x)$. For $x=0$, one has $\varphi=0°$, and, by the time J_0 has reached its first zero at $x=2.405$, φ has monotonically increased to the order of 45°.

A sequence of interference minima occurs on or near the centerline of the "X" shape in Fig. 9 at $\delta\approx 1.0°$, 3.0°, 5.0°, 6.8°, 8.7°, 10.5°, and 12.3°. The last of these coincides with the end of the overlap region of the two surface waves. The locations of the relative minima can be understood as follows. Consider the portion of the overlap region in which $J_0(k_0a\delta)$ can be approximated by its asymptotic form. This occurs when $\delta>0.6°$. The field of the two overlapping surface waves can then be written as

$$\begin{aligned}E^{\text{scatt}}(\pi-\delta)=&\,T(\pi-\delta-\theta_c)B(k,\pi-\delta\\&-\theta_c)\exp[ika\Phi(k,\pi-\delta-\theta_c)]\\&-iT(\pi+\delta-\theta_c)B(k,\pi+\delta\\&-\theta_c)\exp[ika\Phi(k,\pi+\delta-\theta_c)].\end{aligned} \tag{40}$$

The first term in Eq. (40) is the shorter path length surface wave and the second term is the longer path length surface wave. The second term contains an extra factor of $-i$ since it has crossed the backscattering focal line. When Eq. (40) and the Gaussian pulse spectrum of Eq. (5) are inserted into Eq. (2), the Taylor series expansions of B and Φ are truncated at B_0 and Φ_0, and the time-domain intensity is obtained from the time-domain field, the result is

$$\begin{aligned}I^{\text{scatt}}(t,\theta)=&\,W_S^2(t,\theta)\\&+2W_S(t,\theta)W_L(t,\theta)\sin\{k_0a[\Phi(k_0,\pi+\delta-\theta_c)\\&-\Phi(k_0,\pi-\delta-\theta_c)]\}+W_L^2(t,\theta),\end{aligned} \tag{41}$$

where

$$\begin{aligned}W_S(t,\theta)=&\,(k_0a)^{4/3}T(\pi-\delta-\theta_c)B_0(k_0,\pi-\delta\\&-\theta_c)\exp\{-[ct-a\Phi_0(k_0,\pi-\delta-\theta_c)]^2/\sigma^2\},\end{aligned} \tag{42}$$

$$\begin{aligned}W_L(t,\theta)=&\,(k_0a)^{4/3}T(\pi+\delta-\theta_c)B_0(k_0,\pi+\delta\\&-\theta_c)\exp\{-[ct-a\Phi_0(k_0,\pi+\delta-\theta_c)]^2/\sigma^2\}.\end{aligned} \tag{43}$$

Keeping only the dominant portion of Φ_0 in Eq. (28), Eq. (41) simplifies to

$$\begin{aligned}I^{\text{scatt}}(t,\theta)=&\,W_S^2(t,\theta)+2W_S(t,\theta)W_L(t,\theta)\sin(2k_0a\delta)\\&+W_L^2(t,\theta),\end{aligned} \tag{44}$$

which has its relative minima at

$$\begin{aligned}\delta&=(M-1/4)\pi/k_0a\\&=1.40°,3.26°,5.12°,6.98°,8.85°,10.71°,\text{ and }12.57°,\end{aligned} \tag{45}$$

where M is an integer. These values, except perhaps for the first one where the asymptotic form for J_0 may not yet be sufficiently accurate, are in good agreement with the positions of the relative minima in Fig. 9. They are also the approximate locations of the zeros of $J_0(k_0a\delta)$ for monochromatic plane wave incidence.

4. CONCLUSIONS

For many years, researchers have examined light scattering of a pulse of electromagnetic radiation by a small particle in the time domain. Previous studies have almost always concerned themselves with the temporal signal at a single angle. In this paper, we considered time-domain scattering as a function of both time and scattering angle, and for only a single term of the Debye series rather than for the entire Mie sum. Our purpose in doing this was to be able to study various scattering processes from a new point of view. The Debye series separates out most, but not all, of the scattering mechanisms. Of those that remain unseparated, going over to the time domain separates most, but not all, of them. In this paper, after briefly studying the contribution of geometrical rays in the short wavelength limit, we focused on the properties of surface wave radiation for transmission and transmission following

a single internal reflection. We found that time-domain scattering by a short pulse provides a better measurement of the surface wave velocity than is obtained by scattering of a monochromatic plane wave, after the dispersion effects of the pulse have been taken into account. We found that the damping rate of surface wave radiation may be characterized equally well using either type of incidence. The surface wave glory, however, takes on a readily interpretable form in the time domain, and the contributions of the individual surface waves whose interference creates the glory are easily visible. The disentangling of various physical processes is not complete at $\theta = 180°$ since both counterpropagating $p = 1$ surface waves have the same scattering angle and the same path length, and cannot be separated at that one angle in the time domain. Despite this, the separation of the surface wave contributions at every other scattering angle may be easily visualized and interpreted in Figs. 4, 5, and 9.

REFERENCES

1. H. C. van de Hulst, "Rigorous scattering theory for spheres of arbitrary size," in *Light Scattering by Small Particles* (Dover, 1957), pp. 114–130.
2. M. Kerker, "Scattering by a sphere," in *The Scattering of Light and Other Electromagnetic Radiation* (Academic, 1969), pp. 27–96.
3. C. F. Bohren and D. R. Huffman, "Absorption and scattering by a sphere," in *Absorption and Scattering of Light by Small Particles* (Wiley-Interscience, 1983), pp. 82–129.
4. P. Debye "Das Elektromagnetische Feld um einen Zylinder und die Theorie des Regenbogens," in *Geometrical Aspects of Scattering*, P. L. Marston, ed., Milestone Series (SPIE, 1994), Vol. MS89, pp. 198–204.
5. B. Van der Pol and H. Bremmer, "The diffraction of electromagnetic waves from an electrical point source round a finitely conducting sphere, with applications to radiotelegraphy and the theory of the rainbow," Philos. Mag. **24**, 825–864 (1937).
6. E. S. C. Ching, P. T. Leung, and K. Young, "The role of quasinormal modes," in *Optical Processes in Microcavities* R. K. Chang and A. J. Campillo, eds. (World Scientific, 1996), pp. 1–75.
7. R. Greenler, "Rainbows," in *Rainbows, Halos, and Glories* (Cambridge University, 1980), pp. 8–10.
8. L. Mees, G. Gouesbet, and G. Grehan, "Scattering of laser pulses (plane wave and focused Gaussian beam) by spheres," Appl. Opt. **40**, 2546–2550 (2001).
9. L. Mees, G. Grehan, and G. Gouesbet, "Time-resolved scattering diagrams for a sphere illuminated by plane wave and focused short pulses," Opt. Commun. **194**, 59–65 (2001).
10. H. Bech and A. Leder, "Particle sizing by ultrashort laser pulses —numerical simulation," Optik **115**, 205–217 (2004).
11. H. Bech and A. Leder, "Particle sizing by time-resolved Mie calculations—a numerical study," Optik **117**, 40–47 (2006).
12. S. Bakic, C. Heinisch, N. Damaschke, T. Tschudi, and C. Tropea, "Time integrated detection of femtosecond laser pulses scattered by small droplets," Appl. Opt. **47**, 523–530 (2008).
13. P. Laven, "Separating diffraction from scattering: the million-dollar challenge," J. Nanophotonics **4**, 041593 (2010).
14. J. B. Keller, "A geometrical theory of diffraction," in *Calculus of Variations and its Applications*, L. M. Graves, ed., Proceedings of Symposia in Applied Mathematics (McGraw-Hill, 1958), Vol. 3, pp. 27–52.
15. J. A. Lock and P. Laven, "Mie scattering in the time domain. Part 2. The role of diffraction," J. Opt. Soc. Am. A**28**, 1096–1106 (2011).
16. D. Q. Chowdhury, S. C. Hill, and P. W. Barber, "Time dependence of internal intensity of a dielectric sphere on and near resonance," J. Opt. Soc. Am. A **9**, 1364–1373 (1992).
17. E. E. M. Khaled, D. Q. Chowdhury, S. C. Hill, and P. W. Barber, "Internal and scattered time-dependent intensity of a dielectric sphere illuminated with a pulsed Gaussian beam," J. Opt. Soc. Am. A **11**, 2065–2071 (1994).
18. K. S. Schifrin and I. G. Zolotov, "Quasi-stationary scattering of electromagnetic pulses by spherical particles," Appl. Opt. **33**, 7798–7804 (1994).
19. The International Association for the Properties of Water and Steam, "Release on refractive index of ordinary water substance as a function of wavelength, temperature and pressure" (International Association for the Properties of Water and Steam, 1997), www.iapws.org/relguide/rindex.pdf.
20. R. M. Pope and E. S. Fry, "Absorption spectrum (380–700 nm) of pure water. II. Integrating cavity measurements," Appl. Opt. **36**, 8710–8723 (1997).
21. W. J. Wiscombe, "Improved Mie scattering algorithms," Appl. Opt. **19**, 1505–1509 (1980).
22. H. M. Nussenzveig, "High-frequency scattering by a transparent sphere. I. Direct reflection and transmission," J. Math. Phys. **10**, 82–124 (1969).
23. H. M. Nussenzveig, "High-frequency scattering by an impenetrable sphere," Ann. Phys. **34**, 23–95 (1965).
24. M. Abramowitz and I. A. Stegun, eds., "Bessel functions of integer order," in *Handbook of Mathematical Functions* (National Bureau of Standards, 1964), p. 366, Eq. (9.3.3).
25. H. C. van de Hulst, "The reflected and refracted light," in *Light Scattering by Small Particles* (Dover, 1957), p. 212.
26. K. W. Ford and J. A. Wheeler, "Semiclassical description of scattering," Ann. Phys. **7**, 259–286 (1959).
27. M. V. Berry and K. E. Mount, "Semiclassical approximations in wave mechanics," Rep. Prog. Phys. **35**, 315–397 (1972).
28. V. Khare, "Short-wavelength scattering of electromagnetic waves by a homogeneous dielectric sphere," Ph.D. dissertation (University of Rochester, 1975), Eqs. 8.32–8.35, 8.40–8.42.
29. M. Abramowitz and I. A. Stegun, eds., "Bessel functions of integer order," in *Handbook of Mathematical Functions* (National Bureau of Standards, 1964), p. 366, Eq. (9.3.4).
30. M. Abramowitz and I. A. Stegun, eds., "Bessel functions of fractional order," in *Handbook of Mathematical Functions* (National Bureau of Standards, 1964), p. 478, Table 10.13.
31. H. M. Nussenzveig, "Uniform approximation in scattering by spheres," J. Phys. A **21**, 81–109 (1988).
32. H. M. Nussenzveig and W. J. Wiscombe, "Complex angular momentum approximation to hard-core scattering," Phys. Rev. A **43**, 2093–2112 (1991).
33. I. S. Gradshteyn and I. M. Ryzhik, "Definite integrals of elementary functions," in *Table of Integrals, Series, and Products* (Academic, 1965), p. 495, Eq. (3.952.1).
34. H. C. van de Hulst, "Waves at the surface of a perfect conductor," in *Light Scattering by Small Particles* (Dover, 1957), p. 368.
35. H. C. van de Hulst, "Intensity," in *Light Scattering by Small Particles* (Dover, 1957), p. 205.
36. H. C. van de Hulst, "Theory based on Mie's formula," in *Light Scattering by Small Particles* (Dover, 1957), p. 253.
37. V. Khare, "Short-wavelength scattering of electromagnetic waves by a homogeneous dielectric sphere," Ph.D. dissertation (University of Rochester, 1975), Eqs. 8.10, 8.14b.
38. G. Arfken, "Bessel functions," in *Mathematical Methods for Physicists*, 3rd ed. (Academic, 1985), p. 620.
39. H. C. van de Hulst, "Phase," in *Light Scattering by Small Particles* (Dover, 1957), p. 207.